# NUMERICAL ANALYSIS OF PARTIAL DISCHARGE BEHAVIOUR UNDER DC STRESS WITH VOLTAGE DISTURBANCE AT DIFFERENT VOID SIZES

## NUR SHAHIDA MIDI\*, MUHAMMAD ALIF SULAIMAN

Electrical and Computer Engineering Department, International Islamic University Malaysia, Kuala Lumpur, Malaysia

\*Corresponding author: nurshahida@iium.edu.my

(Received: 23 August 2024; Accepted: 24 April 2025; Published online: 15 May 2025)

ABSTRACT: Partial discharge (PD) is commonly related to electrical insulator degradation. It occurs in a high electric field environment, especially in high-voltage systems. It can lead to the electrical breakdown of insulators. Knowledge of the characteristics of PD allows for testing and monitoring of insulation properties in power system equipment. PD can be observed in both AC and DC power. However, research on AC-PD is much more mature than DC-PD due to the established pattern of AC's changing magnitude and polarity characteristics. This work uses finite element analysis to study PD activity under DC stress with voltage disturbance at different void sizes, with AC harmonic as the focused disturbance. The characteristics are evaluated based on the electric potential distribution, electric field distribution, electrical charges, and repetition rate. As the void radius increases from 1 mm to 4 mm, the inception voltage decreases by approximately 65%, while the PD repetition rate increases by 58%. In addition, a comparison between DC-PD and AC harmonic disturbance and AC-PD is performed to analyze their differences. The simulation result shows that the repetition rate for DC-PD with AC harmonics is approximately 75% lower than that of AC-PD, indicating fewer PD events in the case of DC-PD with AC harmonics. The conducted simulation provides valuable insights and guidance for the formation of DC-PD testing, and consequently, a validated method can be approved to monitor insulating material condition under DC power.

ABSTRAK: Penyahcasan separa (partial discharge, PD) merupakan fenomena biasa yang berkait rapat dengan degradasi penebat elektrik. Ia berlaku dalam persekitaran medan elektrik tinggi, khususnya dalam sistem voltan tinggi, dan boleh menyebabkan kerosakan elektrik pada penebat. Pengetahuan mengenai ciri-ciri PD membolehkan ujian dan pemantauan sifat penebat dalam peralatan sistem kuasa dijalankan. PD boleh diperhatikan dalam kedua-dua kuasa arus ulang-alik (AC) dan arus terus (DC). Namun, kajian mengenai PD dalam AC adalah lebih matang berbanding dalam DC disebabkan oleh corak perubahan magnitud dan polariti AC yang telah mapan. Kajian ini meneliti aktiviti PD di bawah tekanan DC dengan gangguan voltan pada saiz kekosongan yang berbeza menggunakan analisis elemen terhingga, dengan gangguan harmonik AC sebagai tumpuan utama. Ciri-ciri yang dinilai termasuk taburan potensi elektrik, taburan medan elektrik, cas elektrik, dan kadar pengulangan. Apabila jejari kekosongan meningkat dari 1 mm kepada 4 mm, voltan permulaan menurun sebanyak kira-kira 65%, manakala kadar pengulangan PD meningkat sebanyak 58%. Selain itu, perbandingan antara PD-DC dengan gangguan harmonik AC dan PD-AC turut dilakukan bagi menganalisis perbezaannya. Hasil simulasi menunjukkan bahawa kadar pengulangan bagi PD-DC dengan gangguan harmonik AC adalah kira-kira 75% lebih rendah berbanding PD-AC, menandakan bilangan kejadian PD yang lebih sedikit dalam kes PD-DC dengan gangguan harmonik. Simulasi yang dijalankan ini memberikan pandangan yang bernilai dan panduan berguna bagi pembentukan ujian PD-DC, dan seterusnya, kaedah yang disahkan boleh diluluskan untuk memantau keadaan bahan penebat di bawah kuasa DC.

KEYWORDS: Partial discharge, DC, AC harmonics, void, FEA

#### 1. INTRODUCTION

In electrical power systems, partial discharge (PD) is the first indication that the insulation properties of an electrical apparatus are deteriorating. The failure of the insulation system can eventually cause the breakdown of the apparatus, jeopardizing the reliability of the transmission and distribution system. PD is an electrical breakdown that occurs in insulating materials caused by operating stresses [1] such as an overhigh electric field [2]. Under normal circumstances, the insulators contain defects such as voids or air-filled gaps that promote the activity of PD. However, PDs do not cause an abrupt breakdown of the insulation property. When subjected to long and harsh operations, insulating properties start to degrade, causing an increase in PD activity, which eventually could lead to total breakdown [3], [4].

PD detection and measurement are known as a standard method to evaluate the quality of the insulation system [5]; where the knowledge of the PDs' characteristics is crucial for their detection and measurement. Various techniques have been developed for PD measurement, analysis, and recognition, particularly for partial discharge under AC stress (AC-PD). AC voltage operation in terms of its polarity and direction changes is naturally made suitable for monitoring PDs. The pure AC output from transformer conversion allows simplicity in measuring the discharge value without any disturbances.

The critical parameters for measurement include partial discharge inception voltage (PDIV) [6] apparent charge, repetition rate, and the Phase-Resolved Partial Discharge (PRPD) pattern [7]. These parameters are highly influenced by the types of insulating materials, voltage stress, temperature, humidity, impurities, and defects (usually referred to as voids) geometry [4], [6], [8]. The knowledge of the fundamental characteristics of AC-PD, combined with information about the parameters, allows for monitoring the insulation properties of the power system apparatus. Current research is also integrating PD simulation modelling and machine learning [9], [10] in facilitating this method of insulation monitoring.

On the other hand, recent developments in high voltage transmission and distribution systems show an increasing interest in high voltage direct current (HVDC) systems. Similar to the traditional HVAC systems, the insulation systems for HVDC also face the same partial discharge (DC-PD) problem. Unlike AC-PD, which is already well characterized, PRPD is well established as a method of analysis; the fundamental characteristics of DC-PD are still not well known. DC power behaves differently from AC power in terms of its electrical characteristics, such as the magnitude, type, and phase. These differences in characteristics are enough to influence the PD behaviours between AC and DC systems. However, the testing and monitoring procedures of DC-PD are still unclear because the study is still being conducted, and researchers are studying and developing new methods for a definitive solution.

This paper aims to contribute to this study by simulating the PD activity under DC stress with voltage disturbance at different void sizes. In relation to DC power, the output transmission voltage in an HVDC system contains voltage disturbances such as traces of AC harmonic voltage or DC voltage ripple. Thus, it is essential to investigate the effect of voltage disturbance on the characteristics of DC-PD. Here, finite element method (FEM) analysis will be used to analyze the DC-PD characteristic for different void size in cross-linked polyethylene (XLPE) material under DC stress superimposed with AC harmonics.

#### 2. METHODOLOGY

This chapter consists of several sections. Section 2.1 covers the model's geometry and the simulation parameters. Section 2.2 shows the governing equation of PD modelling using the FEA method. Fig. 1 shows a summary of the methodology.

#### 2.1. Model Configuration

The model for this simulation uses a 2D axisymmetric dimension, allowing for only half of the geometry to be drawn, with the remainder completed through 3D revolution or 2D mirroring. Fig. 2 shows the model following the CIGRE Method-II (CM-II) Type Metal-Air Gap-Metal Electrode system [11]; comprises an insulator material sandwiched by two electrodes, and a cylindrical-shaped air gap is created in the middle of the insulator. The electrodes' pole is 3mm in radius and 20mm in height, while the electrode plates are 20mm in radius and 2mm in height. The insulator material is 25mm in radius and 2mm in height. The void radius varies as a parameter, taking 1 mm, 2 mm, 3 mm, and 4 mm values.

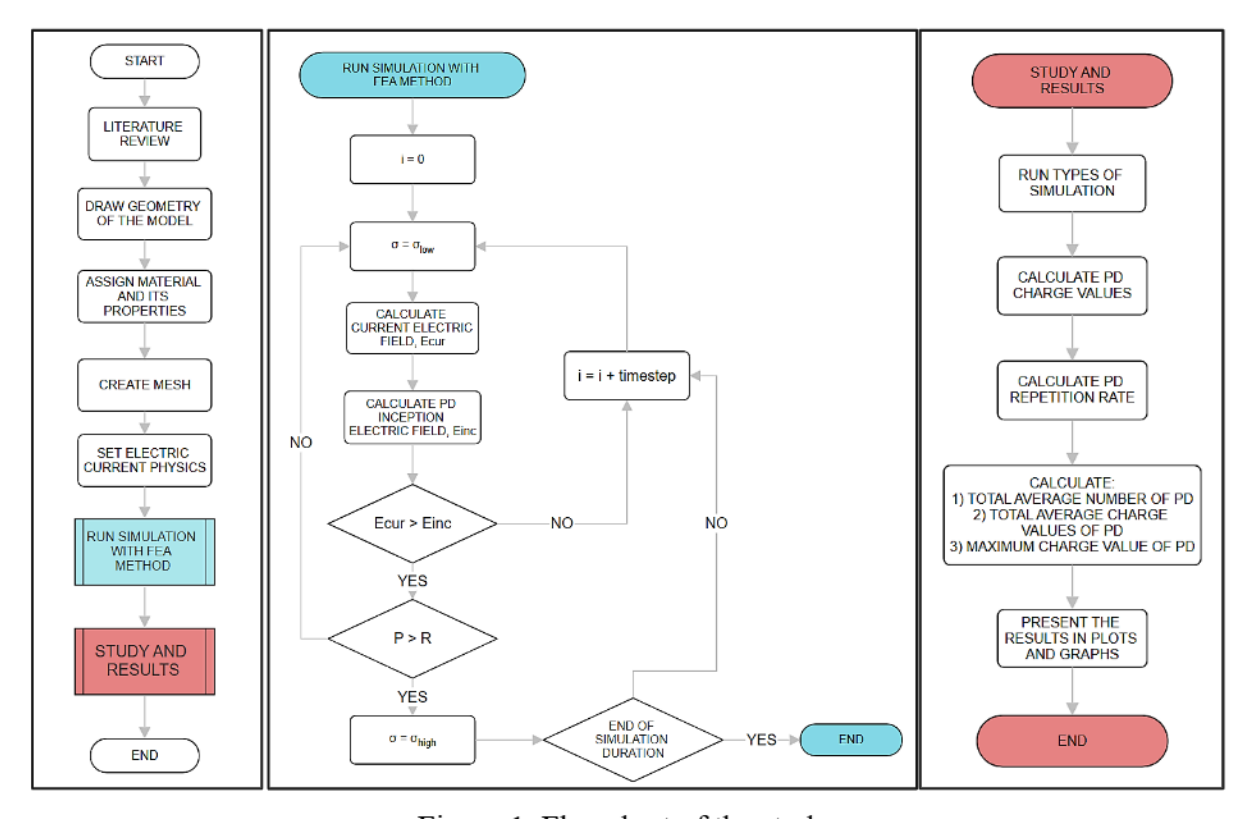


Figure 1. Flowchart of the study.

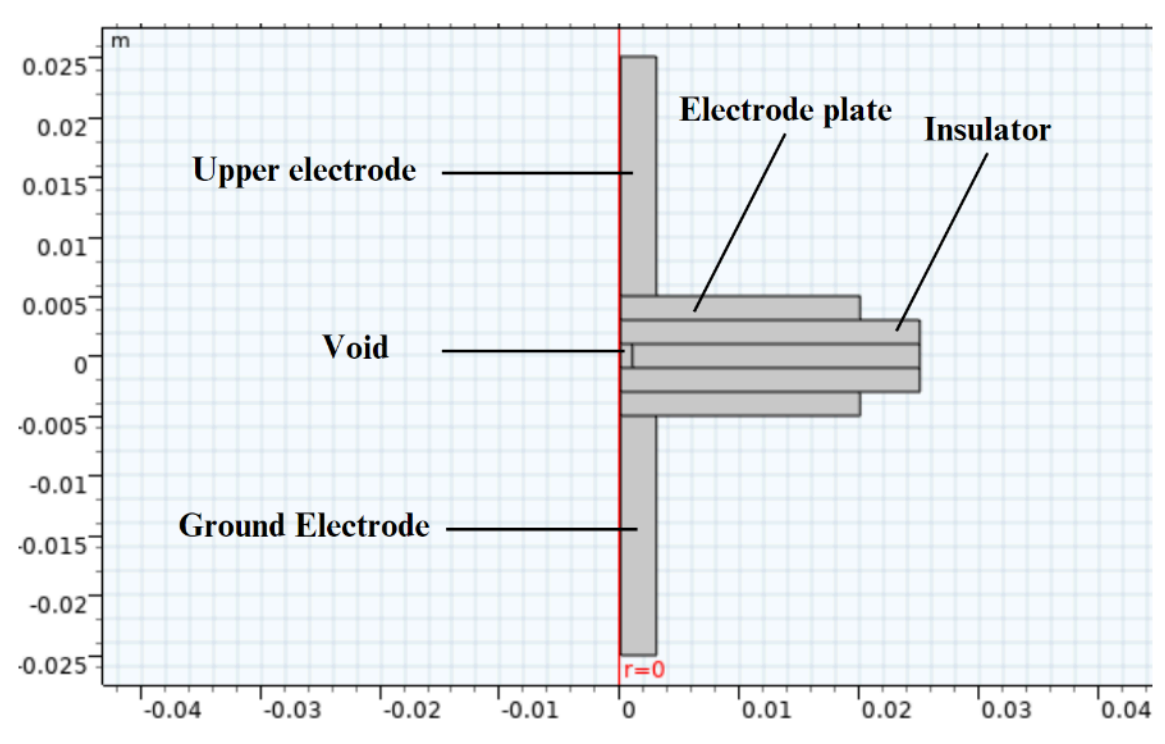


Figure 2. Geometry of the model

Each part of the geometry is assigned materials used experimentally to simulate the partial discharge (PD) model. The electrodes are made of copper metal, suitable for electrical conductivity. The material of the insulator cable is cross-linked polyethylene (XLPE) since this material is often utilized in HVDC systems where the cross-linking by-products, impurities, voids, and gaps can easily cause space charge accumulation under HVDC stress, consequently leading to PD. On the other hand, the material of the void is air [12], with significantly lower dielectric strength than XLPE, a standard material used for PD simulation. Properties of the materials are configured to fulfill simulation requirements, namely the relative permittivity and electrical conductivity, summarized in Table 1. The relative permittivity is the ratio between the absolute permittivity of the insulator and the absolute permittivity of vacuum. At the same time, the electrical conductivity determines the material's ability to conduct electric current. Next, the mesh of the model is created to establish the numerical computation process. Triangular meshing is used for this model, and the mesh element size is set to fine to allow accurate measurement, but this reduces computational resources. Fig. 3 represents the built mesh on the model.

Table 1. Material properties

| Materials | Relative<br>permittivity | Electrical conductivity [S/m] |
|-----------|--------------------------|-------------------------------|
| Copper    | 1                        | 5.998×10 <sup>7</sup>         |
| XLPE      | 2.3                      | $1 \times 10^{-13}$           |
| Air       | . 1                      | 1×10 <sup>-15</sup> (Initial) |

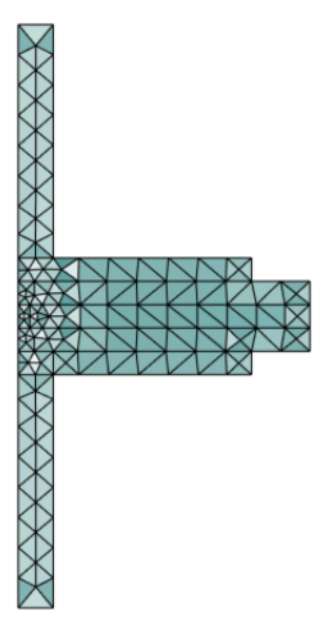


Figure 3. Mesh of the model

Two types of input voltage are defined for the simulations: a) DC input voltage superimposed with AC harmonics and b) AC input voltage. The DC + AC harmonics voltage contains 500kV (DC) + 100kV (AC), while the AC input voltage has a magnitude of 600kV, as shown in Fig. 4.

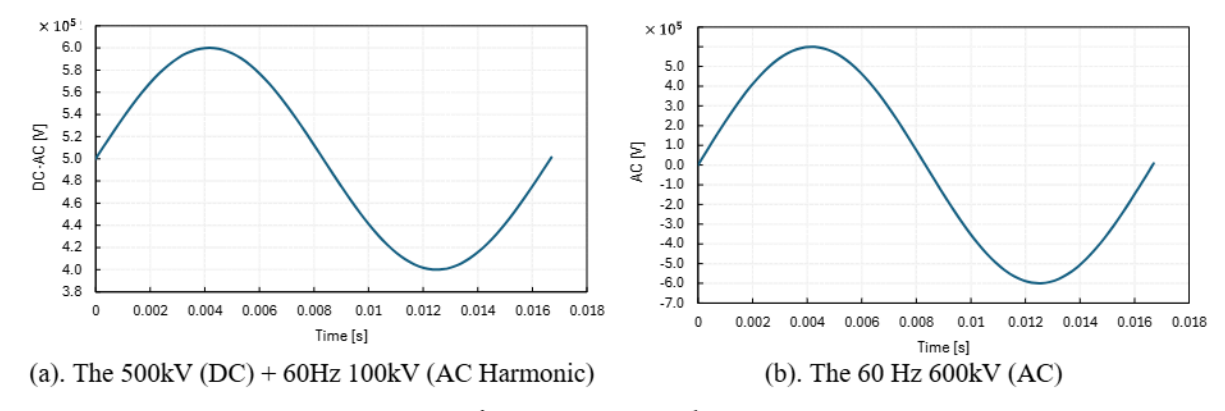


Figure 4. Input voltages

### 2.2. Governing Equations

First, the upper electrode is determined as the terminal to receive the input voltage, while the ground electrode becomes the ground terminal. The assumptions for this analysis are as follows:

- a. The geometry, material properties, and boundary conditions are symmetric about a central axis.
- b. The current continuity equation is satisfied throughout the entire domain.
- c. The electrical insulation is perfect, where no current flows through the insulated boundaries or regions.

The electric potential and electric field distribution are calculated based on the governing equations as follows [13]:

$$\nabla \cdot \mathbf{D} = \mathbf{\rho} \tag{1}$$

$$\sigma E = J \tag{2}$$

$$\nabla J = \frac{\partial \rho}{\partial t} \tag{3}$$

$$D = \varepsilon E = -\varepsilon \nabla U \tag{4}$$

$$J = \sigma E = -\sigma \nabla U \tag{5}$$

$$-\nabla(\sigma\nabla V + \varepsilon\nabla\left(\frac{\mathrm{d}\mathbf{v}}{\mathrm{d}\mathbf{t}}\right) = 0\tag{6}$$

Eq. (1) is Gauss' Law, which states that the total electric flux is equal to the total electric charge across a closed surface. D is the electric flux density,  $\rho$  is the volume charge density and  $\nabla$  is the gradient operator. Eq. (2) is from the derivation of Ohm's Law, and it takes into account the electric field, E, current density, J, and conductivity,  $\sigma$ . The next three are further derivations of the first two, and these equations are translated into Eq. (6).

The first FEA condition of PD occurrence is when the current electric field value,  $E_{cur}$ , inside the void is higher than the minimum inception electric field value,  $E_{inc}$  [14], [15]. This is known as the streamer inception criterion, where the electrons gain energy, perform further ionization in molecules and atoms, and cause an avalanche of excited electrons. The formula for  $E_{inc}$  is represented as follows:

$$E_{inc} = (E_1/p)_{cr} p \left(1 + \frac{B}{(2pa)^n}\right)$$
 (7)

where p is the air pressure inside the void, a is the void radius and  $(E_1/p)_{cr}$ , B and n is parameters that are involved in gas ionizations. The constant values for these parameters are  $(E_1/p)_{cr} = 24.2 \text{ VPa}^{-1}\text{m}^{-1}$ , B = 8.6 Pa<sup>1/2</sup>m<sup>1/2</sup> and n = 0.5. After a period of discharge occurs, the electric field inside the void starts to drop because there is a difference of strength between the electric field left by the charged particles and the supplied voltage. When the value falls below an extinction value  $(E_{ext})$ , the streamer discharge cannot be fulfilled. The formula for  $E_{ext}$  is represented as follows:

$$E_{ext} = p\gamma(E/p)_{cr}$$
 (8)

where y depends on the voltage polarity and is usually obtained from experiments [13].

The second condition is the electron generation rate and the probability of electron availability. Eq. (9) is used to assess the availability of electrons for PD to occur, where  $N_{es}$  is a constant,  $U_{cav}$  is the voltage across void,  $U_{inc}$  is the PD inception voltage across the void, and  $\Delta t$  is the time step of the simulation. Then, in Eq. (10), P is calculated to determine the probability of generating free electrons at the time step of the simulation [16]. Subsequently, P is compared with R, where R is a random number between 0 and 1 (0 < R < 1).

At  $E_{cur} > E_{inc}$  and P > R, PD occurrences are dynamically simulated by switching the void's state from non-conducting to conducting (i.e., increasing the conductivity  $\sigma_{cav}$  from  $\sigma_{low}$  to  $\sigma_{max}$ ), as shown in Eq. (11). This causes the field inside the void to increase again, and the discharges are repeated. Table 2 summarizes the constant parameters implemented in this simulation.

$$\dot{N}_{tot}(t) = N_{es} \exp(|U_{cav}/U_{inc}|) \tag{9}$$

$$P = \dot{N}_{tot}(t)\Delta t \tag{10}$$

$$\sigma_{cav} = \begin{cases} \sigma_{max} & E_{CUR} \ge E_{INC} \& P > R \\ \sigma_{low} & E_{CUR} \le E_{EXT} \end{cases}$$
 (11)

| Symbols        | Parameters                       | Values                                    |
|----------------|----------------------------------|---|
| F              | Frequency of the input voltages  | 60 Hz                                     |
| T              | Period of the input voltages     | 0.0167 s                                  |
| $\sigma_{max}$ | Max conductivity of the void     | $5x10^{-4} \text{ S/m}$                   |
| $\sigma_{low}$ | Min conductivity of the void     | $1x10^{-15}$ S/m                          |
| P              | Void pressure                    | 101325 Pa                                 |
| γ              | Streamer propagation factor      | 0.35                                      |
| $(E/p)_{cr}$   | Gas ionization constant          | 24.2 V. Pa <sup>-1</sup> .m <sup>-1</sup> |
| В              | Gas ionization parameter, air    | 8.6 Pa <sup>1/2</sup> m <sup>1/2</sup>    |
| n              | Gas ionization constant, air     | 0.5                                       |
| $N_{es}$       | Initial electron generation rate | 650 1/s                                   |
| $\Delta t$     | Simulation time step             | -   |

Table 2. Constant parameters of the simulation [13], [16], [17]

PD charge magnitudes and repetition rate are standard parameters used to evaluate PD, and they can be calculated using Eq. (12) and Eq. (13), respectively. It is important to note that the electric field values are taken from the simulation, where only the electric field inception and extinction are considered. Meanwhile, the charge magnitudes and repetition rate are considered in the first condition, and the electron probability is calculated through the electron generation rate formula.

$$q_{real} = \int_{tinc}^{text} \int_{Scav, surf} \vec{J}(t) . \, d\vec{S} dt \tag{12}$$

$$q_{real} = \int_{tinc}^{text} \int_{Scav,surf} \vec{J}(t) . \, d\vec{S}dt \tag{12}$$
 
$$PD \ repetition \ rate = \begin{cases} 1 & E_{CUR} \geq E_{INC} \otimes P > R \\ 0 & E_{CUR} \leq E_{EXT} \end{cases} \tag{13}$$

In Eq. (12), the current density values  $\vec{J}(t)$  is integrated over the  $S_{cav,surf}$  which is the void surface, obtaining the current within the void. Then, the values are integrated again during the interval of PD inception and extinction times. When PD does not occur, the time intervals are flipped and integrated oppositely. The value is recorded at each time step of the simulation. In Eq. (13), the PD repetition rate is counted when the FEA conditions are fulfilled. Only one count is taken for each PD event, which is increased for the next PD event.

#### 3. RESULT AND DISCUSSION

This section covers the results of the DC-PD simulation with AC harmonic disturbance at different void sizes. Section 3.1 shows the electric field distribution of the model and line graphs during the absence and presence of PD. Section 3.2 shows the PD charge magnitudes in a scatter graph and repetition rate in a 2D bar graph. Section 3.3 compares the DC-PD simulation with the AC harmonic disturbance and the pure AC-PD simulation.

#### 3.1. Electric Field Distribution at Different Void Sizes

The influence of AC harmonics disturbance on DC-PD is determined by measuring the electric field. The occurrence of PD is heavily dependent on the electric field values. The plots and values are recorded after simulating one cycle. Fig. 5(a), (b), (c), and (d) indicate that the electric field distribution across all void sizes is uniform, and the voids have lower values than the input voltage. Fig. 5(b), (d), (f), and (h) show the changing electric field values throughout the cycle period. When the electric field PD inception condition is fulfilled, the conductivity changes to a high value. After that, the electric field value drops instantly, fulfilling the PD extinction condition. The conductivity then changes back to a low value, and the electric field value is in accordance with the electric field during the absence of PD. Fig. 5(h) has the highest changing conductivity values because it has the lowest Einc and PD inception voltage, Uinc

value. Thus, the PD inception condition is fulfilled faster in the 4mm void radius simulation than the lower void radius simulations. Table 3 shows the  $E_{inc}$  and  $U_{inc}$  values for each void size simulation.

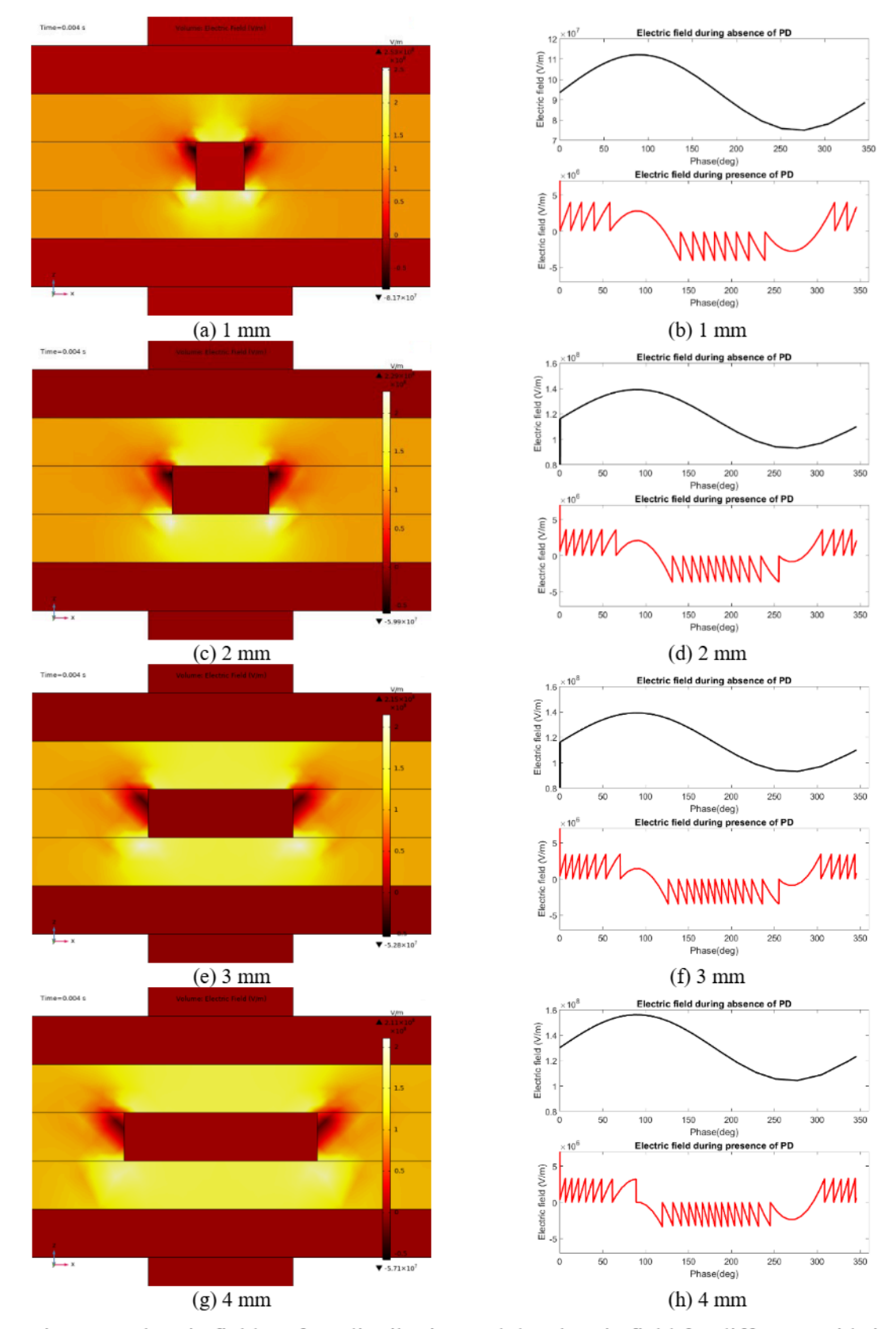


Figure 5. Electric field surface distribution and the electric field for different void sizes

Table 3. The PD electric field and amplitude inception values

| Void radius [mm] | Einc [V/m]           | Uinc [V] |
|------------------|----------------------|----------|
| 1                | $3.93 \times 10^{6}$ | 8499.6   |
| 2                | $3.5 \times 10^{6}$  | 3519.2   |
| 3                | $3.31 \times 10^{6}$ | 3130.6   |
| 4                | 3.19×10 <sup>6</sup> | 2984.5   |

#### 3.2. Evaluation of Electrical Charges and Repetition Rate at Different Void Sizes

The charge magnitude and repetition rate across the void under DC-PD + AC harmonics are calculated for the different void sizes. The value and number of these charges indicate the occurrence of PDs when the conditions for PD are fulfilled. The PD inception and electron generation rate are considered when evaluating the charges. When these conditions are fulfilled, the electrons gain enough energy to move quickly due to the increased electric field strength. This increases the electrical current and, in turn, increases the electrical charges inside the void. The plots and values are recorded after simulating five cycles.

Fig. 6 shows the charge magnitudes and the repetition rate at different void sizes. Fig. 6(e) and Fig. 6(g) show the highest number of PD charges at a high range of charge values. Considering the electron generation rate condition, the increase in void sizes allows the charges to reach very high values. The 3mm and 4mm void size for the PD repetition rate shows the highest number of PDs. Table 4 shows the number of PDs, total charge values, and maximum charge values for each void radius simulation per cycle. The results show that all the parameters increase in value when the void radius increases. As the radius of the void increases, the effective discharge area and the number of charged particles in the discharge channel grow, leading to a higher discharge quantity and increased discharge repetition rate.

Table 4. Evaluation of PD parameters

| Void radius<br>[mm] | Average PD repetition rate per cycle | Average PD charges value per cycle [pC] | Maximum PD charge<br>[pC] |
|---------------------|--------------------------------------|---|---------------------------|
| 1                   | 13.2                                 | 1.3416×10 <sup>3</sup>                  | 5.763×10 <sup>6</sup>     |
| 2                   | 16.8                                 | $2.7851 \times 10^{3}$                  | $4.9488 \times 10^6$      |
| 3                   | 18.2                                 | $3.93 \times 10^{3}$                    | $1.1040 \times 10^7$      |
| 4                   | 20.8                                 | $6.0024 \times 10^3$                    | 1.13862×10 <sup>7</sup>   |

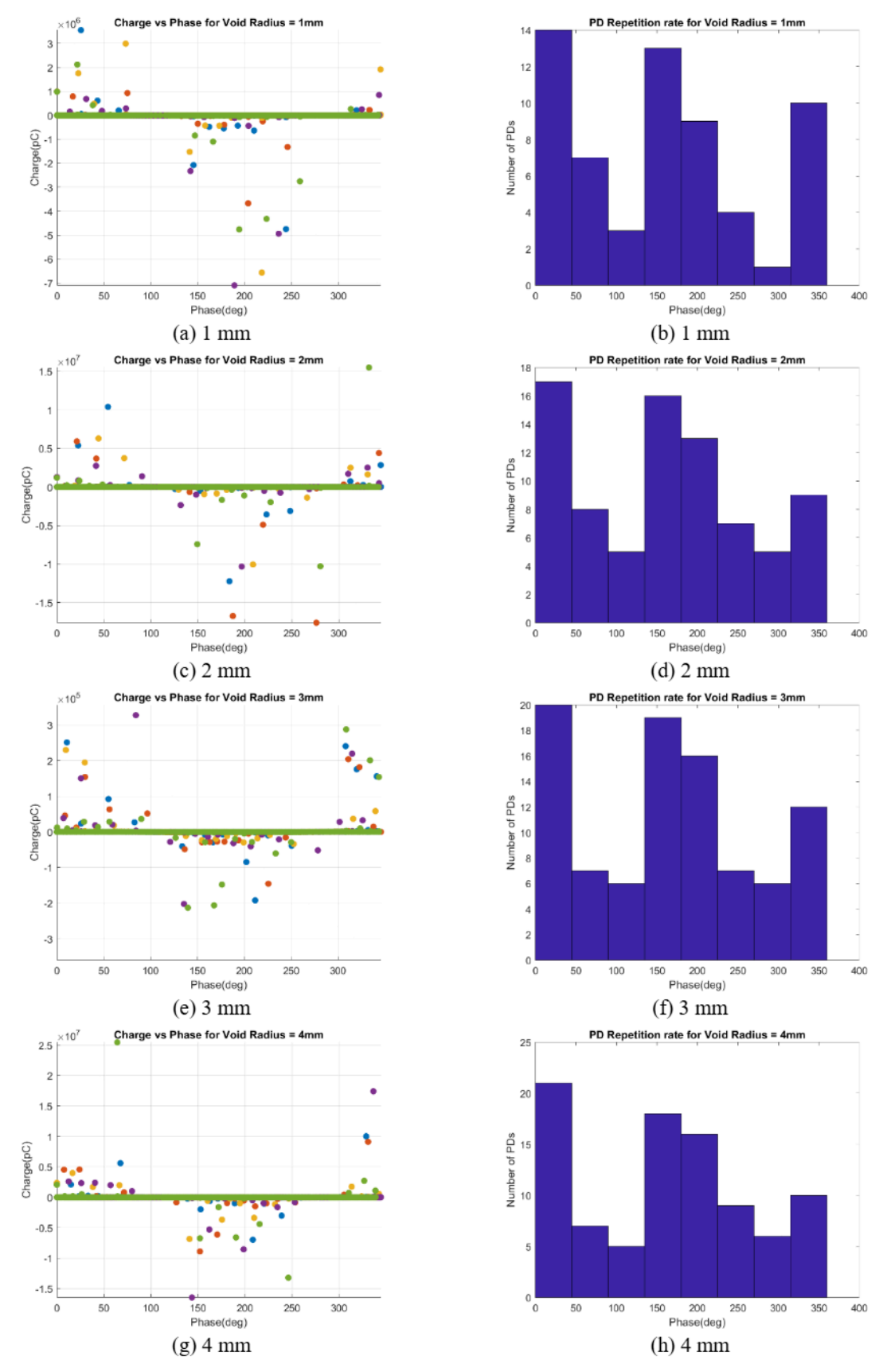


Figure 6. Charge vs phase and PD repetition rate for different void sizes

# 3.3. Comparison of Electrical Charges and Repetition Rate between AC-PD and DC-PD + AC harmonics

After evaluating the simulation characteristics of DC-PD with AC harmonics, the PD behavior between this simulation and the AC-PD simulation is compared to see the differences between these configurations. The void radius is kept constant at 4mm for these comparisons. Fig. 7 displays the PD charges values and repetition rate graph between AC-PD and DC-PD + AC harmonics.

Comparing Fig. 7(a) and Fig. 7(c), the simulations of AC-PD contain a higher range of charge compared to DC-PD + AC harmonics. The comparison of PD repetition rate in Fig. 7(b) and Fig. 7(d) is also significant, where the number of PDs can reach up to 70 counts in AC-PD, while for DC-PD + AC harmonics, it can only reach up to 19 counts. AC-PD possesses a significantly higher average PD repetition rate per cycle than the other simulations. Table 5 shows the recorded PD parameters for the two simulations. This observation might be related to the difference in the input voltages shown in Fig. 5. It can be seen from the figure that amplitudes are different despite the almost similar peak value, indicating a difference in the magnitude of the voltage. AC's input voltage is higher than the DC+AC harmonics, suggesting a higher electric field in the case of AC-PD. However, the average and maximum PD charges in the DC-PD+AC harmonics simulation are not that different from those in the AC-PD simulation. Even though the number of PDs is lower in DC-PD compared to AC-PD, the AC harmonic component of the combined voltage can cause higher PD charge values due to the increase in electric field when the AC values change alternately.

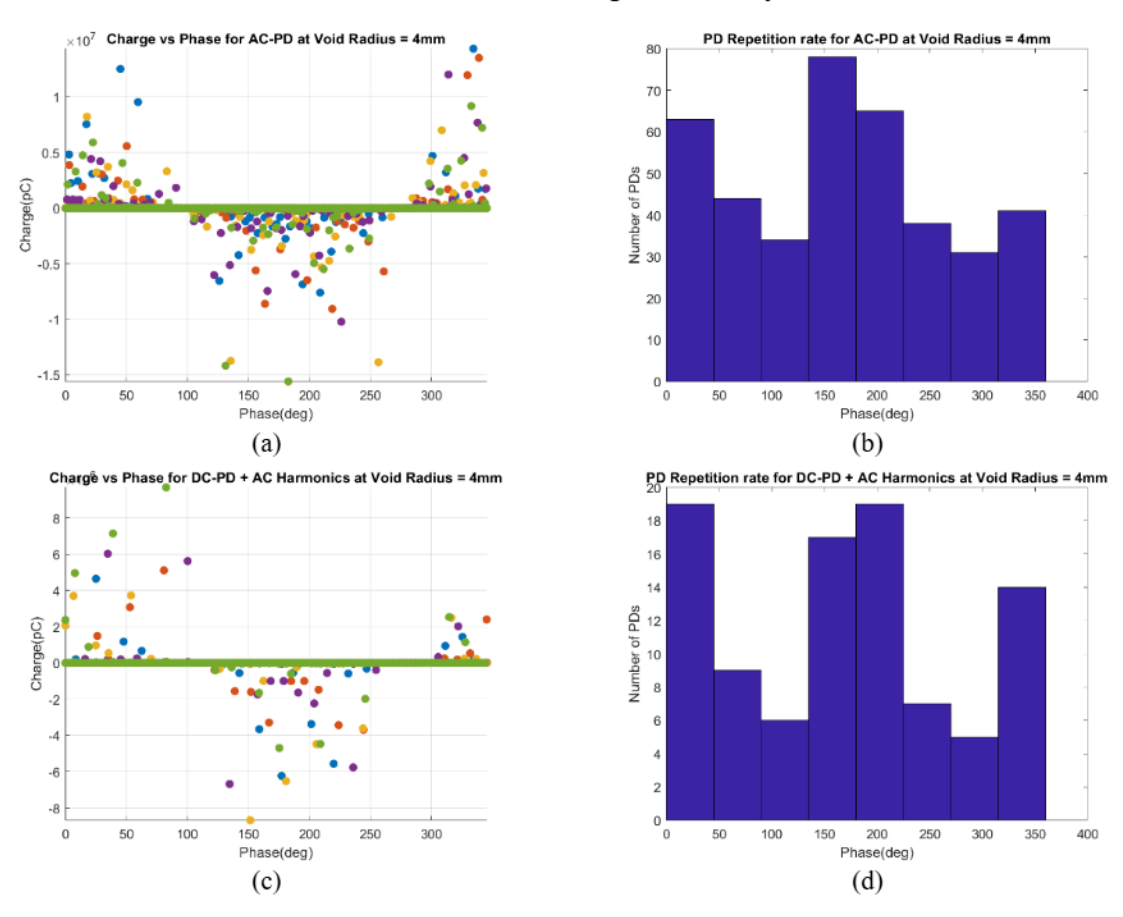


Figure 7. The charge and PD repetition rate at 4mm radius void: (a)(b) AC-PD and (c)(d) DC-PD + AC harmonics

Table 5. Results evaluation of PD parameters between AC-PD and DC-PD with AC harmonics

| Simulation type      | Average PD repetition rate per cycle | Average PD charges value per cycle [pC] | Maximum PD<br>charge [pC] |
|----------------------|--------------------------------------|---|---------------------------|
| AC-PD                | 78.8                                 | $3.1083 \times 10^6$                    | 1.4345×10 <sup>7</sup>    |
| DC-PD + AC harmonics | 19.2                                 | $1.8881 \times 10^{6}$                  | $9.6837 \times 10^6$      |

#### 4. CONCLUSION

PDs are temporary electrical connections that occur between the surface of the insulator and the conductor in high electric fields and voltage systems. Monitoring the condition of the insulator is vital to recognizing the defects. Compared to AC-PD testing, monitoring PD under DC power is not well-developed. Thus, research and study are conducted to unveil new methodologies to improve the monitoring of DC-PD. For simulation, FEA modelling is discovered as one of the methods to model the PD behavior using conditions such as electric field inception, electron generation rate, and the availability of electrons.

The simulation of DC-PD with AC harmonic disturbance has been conducted under different void sizes. The electric field at the void origin is plotted, and the results show that the values change in accordance with the electric field PD inception and extinction conditions at each void size. The inception voltage decreases by approximately 65% with the increase in the radius from 1mm to 4mm. After that, the evaluation of PD charges and repetition rate is recorded. As the void size increases, the charge values and number of PDs also increase, with the maximum charge PD charge increasing by 95% and the average PD repetition rate per cycle increasing by 58%.

A comparison of AC-PD and DC-PD with AC harmonic is performed to view the performance of the testing PDs in these two simulations. It is concluded that AC-PD shows higher values compared to the DC-PD + AC harmonic simulation, where the repetition rate for DC-PD with AC harmonics is approximately 75% lower than that of AC-PD, indicating fewer PD events in the case of DC-PD with AC harmonics.

The simulation of DC-PD with AC harmonics across all simulations provides promising results for observing PDs. At the very least, PDs appear in DC-PD + AC harmonic simulation because the number of PD occurrences is very low in pure DC-PD testing. To conclude, the simulation is successful as the occurrence of PDs is obtained through the combination of DC voltage + AC harmonic disturbance. The simulation provides valuable insights and guidance for developing DC-PD testing and monitoring techniques for assessing the condition of insulating materials. Further research under varying environmental conditions, such as temperature fluctuations and thermal stress, can enhance the application of these methods. Additionally, the DC-PD behavior of various materials used in HVDC facilities, including emerging insulator materials like High-Performance Thermoplastic Elastomer (HPTE), should be further explored. This will help further expand the applicability and understanding of DC-PD behavior in insulating materials.

#### ACKNOWLEDGEMENT

This is supported by the Ministry of Higher Education (MoHE) Malaysia through the Research Management Centre, International Islamic University Malaysia (IIUM) under the Fundamental Research Grant Scheme FRGS (Ref: FRGS/1/2023/TK07/UIAM/02/5– Project ID: FRGS23-320-0929)

#### REFERENCES

- [1] Seri P *et al.* (2019) Partial discharge inception voltage in DC insulation systems: A comparison with AC voltage supply. 2019 IEEE Electrical Insulation Conference, EIC 2019. 176–179. https://doi: 10.1109/EIC43217.2019.9046630
- [2] Zhang X *et al.* (2021) Review on detection and analysis of partial discharge along power cables. https://doi: 10.3390/en14227692
- [3] Borghei M, Ghassemi M, Kordi B, Gill P, Oliver D. (2021) A finite element analysis model for internal partial discharges in an air-filled, cylindrical cavity inside solid dielectric. 2021 Electrical Insulation Conference, EIC 2021. 260–263. https://doi: 10.1109/EIC49891.2021.9612268
- [4] Du Y, Li Y. (2022) Discharge characteristics of epoxy resin partial discharge under different harmonic voltages. 2022 9th International Forum on Electrical Engineering and Automation, IFEEA 2022. 728–731. https://ddoi: 10.1109/IFEEA57288.2022.10037812
- [5] Hussain GA, Hassan W, Mahmood F, Shafiq M, Rehman H, Kay JA. (2023) Review on partial discharge diagnostic techniques for high voltage equipment in power systems. IEEE Access. 11. 51382–51394. https://doi: 10.1109/ACCESS.2023.3279355
- [6] Sahlen F, Takala M. (2023) Factors influencing the partial discharge inception voltage in Type I insulation systems. 2023 IEEE Electrical Insulation Conference, EIC 2023. 1-4. https://doi: 10.1109/EIC55835.2023.10177313
- [7] Mohamed Asseri MA, Hezri Fazalul Rahiman M, Halim Abdul Majid MH. (2022) Partial discharge monitoring and analysis using phase resolve partial discharge pattern. 2022 IEEE 10th Conference on Systems, Process and Control, ICSPC 2022 – Proceedings. 231–235. https://doi: 10.1109/ICSPC55597.2022.10001739
- [8] Montanari GC, Shafiq M, Chen Z. (2024) A discussion on the dependence of partial discharge inception voltage on supply voltage waveform: sinusoidal and modulated AC. 2024 IEEE Electrical Insulation Conference, EIC 2024. 392–396. https://doi: 10.1109/EIC58847.2024.10579408
- [9] Ding B et al. (2021) Pattern recognition of partial discharge based on deep learning. The 16th IET International Conference on AC and DC Power Transmission (ACDC 2020). 1187–1191. https://doi: 10.1049/ICP.2020.0223
- [10] Banjare HK, Sahoo R, Karmakar S. (2022) Study and analysis of various partial discharge signals classification using machine learning application. Proceedings of 2022 6th International Conference on Condition Assessment Techniques in Electrical Systems, CATCON 2022. 52–56. https://doi: 10.1109/CATCON56237.2022.10077703
- [11] Sakakibara T, Kawashima T, Hozumi N, Murakami Y. (2023) Measurement of spark discharge inception voltage using CIGRE Method-II Type metal-air gap-metal electrode system. Proceedings of the International Symposium on Electrical Insulating Materials. 285–287. https://doi:10.23919/ISEIM60444.2023.10329272
- [12] Lagrotteria G, Pietribiasi D, Marelli M. (2019) HVDC Cables The technology boost. 2019 AEIT HVDC International Conference, AEIT HVDC 2019. https://doi: 10.1109/AEIT-HVDC.2019.8740645
- [13] Musa U *et al.* (2023) FEA-based simulation of accelerated ageing in a power cable due to sustained partial discharge activities in a spherical cavity. Arab J Sci Eng. 48(11). 15029–15043. https://doi: 10.1007/S13369-023-07967-7/TABLES/4
- [14] Borghei M, Ghassemi M, Rodriguez-Serna JM, Albarracin-Sanchez R. (2021) A finite element analysis and an improved induced discharge concept for partial discharge modeling. IEEE Transactions on Power Delivery. 36(4). 2570–2581. https://doi:10.1109/TPWRD.2020.2991589
- [15] Rodríguez-Serna JM, Albarracín-Sánchez R, Dong M, Ren M. (2020) Computer simulation of partial discharges in voids inside epoxy resins using three-capacitance and analytical models. Polymers 2020. 12(1). 77. https://doi: 10.3390/POLYM12010077

- [16] Haiba AS, Elfaraskoury AA, Elkoshairy AD, Halawa MM. (2022) Modeling and simulation of partial discharge measurement for defected solid dielectrics. Journal of Measurement Science and Applications (JMSA). 2(1). 43–53. https://doi: 10.21608/JMSA.2022.219865
- [17] Saghafi M, Ghassemi M, Lehr J, Borghei M, Kordi B, Oliver D. (2022) A finite element analysis model for internal partial discharges under DC voltage. 2022 IEEE International Power Modulator and High Voltage Conference, IPMHVC 2022. 8–11. https://doi: 10.1109/IPMHVC51093.2022.10099411